Hydrous mantle melting controls gold enrichment in Kermadec arc magmas

Christian Timm

chrtimm@geomar.de

GEOMAR Helmholtz Centre for Ocean Research

Maxim Portnyagin

GEOMAR https://orcid.org/0000-0001-5197-6562

Cornel de Ronde

GNS Science

Mark Hannington

University of Ottawa

Dieter Garbe-Schönberg

CAU Kiel University, Institute of Geosciences

Kaj Hoernle

GEOMAR Helmholtz Center for Ocean Research Kiel https://orcid.org/0000-0002-3165-3480

Philipp Brandl

GEOMAR Helmholtz Centre for Ocean Research Kiel https://orcid.org/0000-0001-6863-5262

Daniel Layton-Matthews

Queen's University

Matthew Leybourne

https://orcid.org/0000-0002-2361-6014

Richard Arculus

Australian National University https://orcid.org/0000-0002-3432-392X

Article

Keywords:

Posted Date: July 12th, 2024

DOI: https://doi.org/10.21203/rs.3.rs-4680224/v1

Additional Declarations: There is **NO** Competing Interest.

Abstract

Many economic gold deposits on Earth are associated with volcanic arcs. However, little is known about the factors that control the gold endowment of the parental arc magmas. Here, we present new high-precision geochemical data from submarine glasses recovered from the length of the Kermadec arc. We show that the combined systematics of Au, Ag and Cu helps to decipher sources and processes responsible for Au enrichment in arc magmas. These data show that hydrous melting in the Kermadec subarc mantle occurs predominantely at high temperatures in the presence of sulfide liquid. The highest Au (>8 ppb at MgO> 5 wt.%), Au/Cu (up to $6*10^{-6}$) and mantle-like Ag/Cu values correspond to high-temperature second-stage melting. Elevated temperatures in a hydrous subarc mantle enables enhanced and multiple-stage melting of highly depleted mantle and thus is a prerequisite of Au enrichment in parental arc magmas.

Introduction

Some of the largest and highest-grade Au deposits associated with Cu- and Ag-rich mineralization (i.e., epithermal, porphyry copper, volcanic hosted massive sulfides) are found above zones of plate convergence, or subduction zones[1,2]. Evolved magmas generated in subduction zones are enriched in Au, indicating a genetic link between parental magma compositions and gold endowment[3-7]. Gold has a strong affinity for sulfide phases during mantle melting and subsequent magma fractionation [e.g., 8-10]. In the absence of sulfide, Au behaves as an incompatible element with respect to common silicate phases and is concentrated in silicate melts [11]. Many studies have recognized a key role for prolonged sulfide undersaturated crystallization in generating magmas enriched in Au and other strongly chalcophile elements, such as Cu and Ag [e.g., 6,10]. However, it remains controversial whether parental subduction-related magmas are more enriched in Au than, for example, mid-ocean ridge basalts, and if so, what the major factors are that control this enrichment.

The extent to which sulfide is completely consumed during mantle melting, releasing Au to the magma, depends on the degree of melting and the sulfur solubility in the melt at given physical conditions (P, T, fO_2) in the mantle, and on the composition of the melt [6,12-13]. Variations in the degree of partial melting and melting conditions may therefore represent some of the dominant factors controlling the magmatic Au, as well as Ag and Cu inventory[14-17]. Additional factors controlling the Au endowment of parental mantle magmas could be variations in the subarc mantle depletion due to previous episodes of melting [8, 17-18] and, potentially, input of Au-bearing fluids/magmas from the subducting plate [19, 20]. The Kermadec Arc provides a useful case study to isolate the different processes occurring in the sub-arc mantle that influence the Au budget beneath intraoceanic arcs, because variably depleted and enriched mantle sources are involved in magma generation and the angle, composition and thickness of the subducting Pacific Plate changes from thin oceanic crust at the northern segment to thick Hikurangi igneous plateau (LIP) crust beneath the southern segment.

Geological Background

The intraoceanic Kermadec arc and Havre Trough represent an ~1300 km-long arc-backarc system located between New Zealand and Tonga (~25˚S to ~36˚S; Fig. 1). Dehydration of the Pacific Plate, subducting westward beneath the Indo-Australian Plate, drives arc magmatism and the formation of arc front volcanoes, most of which host active hydrothermal systems and some massive sulfide mineralization with high grades of Au[2,23-24]. Arc-related porphyry-, epithermal- and volcanic-hosted sulfide deposits account for a significant proportion of global gold production [25], a number of which originated at submarine arcs in intraoceanic subduction environments. The significance of magmatically-derived precious metals and Cu in active submarine arcs has recently been demonstrated in the Kermadec arc (e.g., Brothers and Clark Seamounts[24,26]). At Brothers Volcano, the main zone of mineralization extends over an area of at least 600 x 200 m with alteration measured (by magnetics) to ~450 m below the seafloor with Au grades of up to 90 ppm Au occuring in some chimneys[24,27]. Submersible dives have been conducted on 14 hydrothermally-active volcanoes of the Kermadec Arc with four of the volcanoes (29%) found to host massive sulfide mineralization. The majority of the Tonga-Kermadec arc volcanoes, however, have not been surveyed in any detail thus the number that host massive sulfides may be higher. What ultimately controls the magmatic Au content remains unclear, yet the sub-arc mantle and its interplay with the subducted Pacific Plate (uppermost lithospheric mantle, altered oceanic crust and sediment veneer) likely plays a significant role. At the Tonga-Kermadec trench, the incoming Pacific Plate changes markedly in thickness and composition from north to south, with the Hikurangi Plateau - a ~9-15 km thick Cretaceous LIP - presently subducting south of ~34.5˚S[27]. To the north of this latitude, ~6 km thick typical oceanic crust comprises the uppermost part of the subducting Cretaceous Pacific Plate. South of 34.5˚S, where the oceanic Hikurangi Plateau subducts beneath the southern Kermadec arc, the total volume of erupted lava is the greatest (~1200 km^3, compared with ~830 km^3 north of 34.5˚S), and the volcano spacing is lowest (~30 km, compared to ~55 km to the north) [2]. Furthermore, the slab surface models from the United Stage Geological Survey [28],derived from relocated seismic events and from ocean bottom seismometer wide-angle refraction seismic data[29], show that the angle of the subducting Pacific Plate changes from ~30˚at ~60 km depth to 47˚at ~100 km depth beneath the northern Kermadec Arc to 20˚at ~60 km depth to 56˚ at ~100 km depth beneath the southern Kermadec arc (Fig.1). The Pacific slab surface beneath the arc front volcanoes, however, remains relatively constant between ~100 and 120 km depth. Lavas from the Kermadec Arc show a marked increase in radiogenic Pb, and to a lesser extent in $^{87}Sr/^{86}Sr$, and a decrease in $^{143}Nd/^{144}Nd$ isotope ratios south of ca. 32°S, interpreted as increased material flux from the subducting Hikurangi Plateau and/or sediments derived from New Zealand [30] or a different ambient mantle composition [e.g., 31].

Volcanic Glass Composition

The composition of the Kermadec arc glasses range from basaltic to rhyolitic and fall into the low-K tholeiitic to medium-K calc-alkaline series (see Table 1; Supplementary File 1). Mafic Kermadec arc

glasses (MgO >5 wt.%) have FeO^t and Au contents similar to, or higher than, mid-ocean ridge basalts (MORB; Fig. 2). Decreasing MgO, Ni and Cr contents with slightly increasing SiO_2 content in the mafic to intermediate glasses (MgO ~3 wt.%) are consistent with predominantly olivine (± pyroxene and plagioclase) crystallization (not shown). Similarly, with decreasing MgO, FeO^t (and TiO_2) decrease abruptly at MgO of ~4 wt.%, suggesting the onset of magnetite (± ilmenite) crystallization, when FeO^t (and TiO_2) are more rapidly removed from the melt [6] (Fig. 2A). Gold contents correlate broadly with FeO^t and show a similar trend of increasing Au content with decreasing MgO from 5 to 3 to wt.% and then decreasing Au at MgO less than 3 wt.%. In samples with MgO > 5 wt.%, Au contents, however, vary by a factor of up to seven and suggest a significant difference between Kermadec volcanoes and parental Au contents or conditions of crustal evolution (Fig. 2B). Copper and Ag behave qualitatively similar (Supplementary File 2), which is generally consistent with fractionation of silicate minerals from sulfide undersaturated melt. The drop in Cu and Au contents at MgO of ~3-5 wt.% is related to sulfide saturation and strong partitioning of these elements into sulfide phases[e.g., 6]. Of note is that sulfide saturation likely occurs at different MgO contents for different volcanoes, suggesting that melt sulfur solubility beneath the volcanoes varies along the arc, most likely due to variable fO_2 or melt composition [38].

Values of Ag/Cu and Au/Cu for Kermadec arc and Havre Trough backarc glasses (with MgO >3 wt.% prior to the onset of magnetite crystallization) show a significant range: Ag/Cu = 2.2-5.8*10^{-5} and Au/Cu= 1.1-6.0*10^{-6}. These values exceed those of mid-ocean ridge basalts (average Ag/Cu~3.0*10^{-5} and Au/Cu = 1.7*10^{-6}[36-37]) and depleted mantle (Ag/Cu~2.7*10^{-5} [39] and Au/Cu ~3.3*10^{-6}[39]). Between 8 and 3 wt.% MgO, Au/Cu and Ag/Cu values show little variation, consistent with no, or little sulfide fractionation during early magma crystallization. The variations of Au/Cu and Ag/Cu in primitive glasses are therefore likely to resemble those in primary magmas. At MgO contents lower than ~3 wt.%, both Au/Cuand Ag/Cu values increase sharply (Fig. 2C and 2D) suggesting segregation of low temperature monosulfide solid solution (MSS), such as Cu-rich phyrrotite [33], cubanite, chalcopyrite or bornite [6].

When plotted against Nb/Zr (and Zr/Hf), a proxy of mantle source depletion and degree of melting, Au/Cu in Kermadec arc glasses shows a broad negative correlation (cf. Fig. 3A). Of note is that glasses from the northern Kermadec arc volcano Putoto have high Au/Cu and the lowest Nb/Zr values indicating that these melts either originate from the most depleted subarc mantle, or underwent the highest degree of partial melting or both. The derivation of of the Putoto samples from most depleted source is also supported by some of the lowest $^{143}Nd/^{144}Nd$ ratios of all Kermadec arc lavas [31]. In addition, glasses from the volcanoes Kibblewhite, Ngatoroirangi, Kuiwai and Rumble III have elevated Au and high Au/Cu at intermediate Nb/Zr, whereas glasses from the Havre Trough basin show no clear correation between Au/Cu and Nb/Zr. Similarly, Ag/Cu in the Kermadec arc and Havre Trough backarc glasses shows no clear correlation with Nb/Zr. The Havre trough glasses, however, form two groups: one with high Nb/Zr, low Au/Cu and MORB-like Ag/Cu and the other with low Nb/Zr, Ag/Cu but high Au/Cu (cf. Fig. 3). High Au/Cu back-arc sample-locations are relatively close to the arc front, therefore resembling arc-front rather than backarc compositions. With the exception of three high-Mg andesite

glasses from Kibblewhite [36] with high Ag/Cu values of ~6 at intermediate Nb/Zr, pointing towards a less depleted parental subarc mantle, most glasses have MORB-like Ag/Cu values of ~ 2-4 (Fig. 3B). Gold contents and Au/Cu values in most mafic Kermadec arc front glasses are higher than Au contents and Au/Cu in MORB either indicating the addition of slab-derived Au to the mantle wedge or mantle melting conditions favoring the generation of Au-rich magmas.

Does gold come from the subducting slab?

Gold can be highly mobile in aqeous fluids as a range of bisulfide, chloride and polysulfide ions[19]. As the trisulfur radical S_3^- can be stable in aqueous fluids up to ~700˚C and ~3.5 GPa [18,45], some of the Au in the sub-arc mantle may therefore have been added by aqueous fluids from the subducting slab. Up to 2.8 wt.% H_2O and ~20-80% sulfate (S^{6+}) in olivine-hosted melt inclusions from the southern Kermadec arc [32] support that H_2O is a (prominent) constituent in the subarc mantle, and that these melts originate from a hydrated and oxidized subarc mantle. Thus, the origin of the Au enrichment via recycling Au by hydrous slab components will be examined below.

Previous studies recognized that slab-related components in Kermadec arc lavas originate from three major sources: subducted sediments, altered MORB-like oceanic crust north of ~34.5°S, and altered LIP crust to the south [31, 46-47]. Strontium and Pb-isotopic compositions require the addition of <1 to ~4 % of a sedimentary component from the subducted Pacific Plate [31].This sedimentary imprint generally increases from north to south, suggesting that the southern Kermadec subarc mantle has been influenced by greater amonts of sediment-derived Sr and Pb than the northern Kermadec subarc mantle. The more radiogenic Sr and Pb isotopic compositions have previously been attributed to the increase in subducting sediment thickness and its composition [46] and to the input from the subducting Hikurangi Plateau[48].

The average Au, Ag and Cu contents in oxic and suboxic seafloor calcareous and biogenic sediments, which comprise the most abundant ocean floor sediments is ~1 ppb Au, ~3 ppb Ag and ~75 ppm Cu [49-52]. These low concentrations are unlikely to change the Au, Ag and Cu contents of the subarc mantle, assuming that 1-4% sediments are present in the mantle wedge and partitioning between slab and fluid is close to unity for these metals. However, sediments formed in anoxic environments, such as sulfide-rich black shales, may contain up to ~7 ppb Au, >1000 ppb Ag and >1000 ppm Cu [49-50, 53], and, if they were subducting beneath the Kermadec arc, could potentially contribute significant amounts of chalcophile elements to the sub-arc mantle. Thus, in order to test whether slab-derived sediment plays a role in supplying Au (plus Ag and Cu) to the Kermadec subarc mantle, we plotted Au, Au/Cu and Ag/Cu against Th/La (a proxy used to detect slab-derived sedimentary component [54]; Supplementary File 3). Au/Cu and Ag/Cu show no systematic trends with Th/La, which precludes large contributions of Au, Ag and Cu from the slab to the overlying mantle wedge from anoxic sediments, consistent with their absence in drillcores from the Hikurangi Plateau offshore New Zealand (IODP Expedition 375) and DSDP site 204 west of the northernmost Kermadec arc [55, 47]. In addition, carbon-isotopes indicate a prevailing

oxic environment in the Pacific Ocean, In addition, the degree of pyritization [56] provides further support of the absence of anoxic sediments in the Pacific region.

Devolatilization of altered oceanic crust may also play an important role in transferring precious metals and Cu to the overlying mantle wedge. For example, Hannington [52] has shown that hydrothermal processes at the East Pacific Rise has led to local Cu enrichments of up to ~10 wt%. Although some LIPs have high Au, Ag and Cu contents (e.g., Tamu Massif at the Shatsky Rise), they contain on average 3.8 ppb, 49 ppb and 178 ppm, respectively[59]. Elevated average Cu contents of 233 ppm have been measured in the Hikurangi basement lavas (i.e., Rapuhia scarp [30]), consistent with the general enrichment in chalcophile elements of LIP crust. In addition, according to Jenner and O'Neill (2012) [38] average global MORBs have Au = 1.4 ppb, Ag = 24 ppb and Cu = 85 ppm and thus are relatively depleted compared to LIP crust. But does the subducting Hikurangi LIP crust supply significant amounts of chalcophile elements to the sub-arc mantle?

A common indicator of the fluid flux from altered oceanic crust is Ba/Th [60], which shows a crude positive correlation with Au/Cu (Fig. 3C). The highest Au/Cu values are, however, found in glasses from the northern Kermadec arc volcano Putoto, which is a long ways north of the subducting Hikurangi Plateau, and thus cannot be related to Au-rich LIP source fluids. In addition, Ba and Th contents in glasses from Putoto are low compared to those from the southern Kermadec arc volcanoes, suggesting fluid is derived from MORB-like and relatively Au-depleted altered oceanic crust. The high Ba/Th and Au/Cu values for Putoto volcano also correspond to very low Nb/Zr (and Zr/Hf) (cf. Fig. 3). It is thus plausible that the distinctive Putoto compositions reflect the most extensive melting of the most depleted mantle. The overall low concentration of Ba and Th, together with very low Nb/Zr (and Zr/Hf and whole rock $^{143}Nd/^{144}Nd$) in these glasses points to high degrees of melting of a depleted mantle wedge rather than a source of Au from slab-derived fluids. High Au/Cu values are also observed in glasses from the Giggenbach, and the southern Kermadec arc volcanoes Kibblewhite, Ngatoroirangi and the southern Havre Trough. Within the southern Kermadec arc these glasses also have some of the lowest Nb/Zr values, consistent with their derivation from the most depleted portions of the southern Kermadec subarc mantle or high degrees of melting.

In summary, there is little evidence for a significant contribution of Au (and Ag and Cu) from the subducting slab, suggesting a predominant mantle control on the Au budget of the Kermadec sub-arc mantle.

Mantle control on gold systematics

The generation of parental arc magmas with high Au contents and Au/Cu can be explained by two scenarios: 1) low-temperature mantle melting with high fractions of mono sulfide solid solution (MSS) present in the source [12], or 2) high-temperature melting of a highly depleted mantle source in the presence of sulfide liquid [8].

Both scenarios are based on experimental studies that show that Au, Ag and Cu have fundamentally different partion coefficients between the melt and sulfide liquid stable at high temperatures of 1300°C, and MSS stable at lower mantle temperatures of 1175-1200°C [12-13]. At temperatures of ≤1200°C, compatibilities between MSS and mantle melts are in the order Cu>Au>Ag, resulting in higher Ag/Cuthan Au/Cu values at low degrees of partial melting [12-13] (see Fig. 4 and Supplementary file 3). At high-temperatures of ≥1300°C, compabilities between sulfide liquid and mantle melts is in the order Au>Cu»Ag resulting in low Au/Cu and mantle-like Ag/Cu values during incipient melting. Values of Au/Cu and Ag/Cu can therefore be used to determine which sulfide phase is stable in the mantle and whether melting occurred at high or low temperatures. According to Zhang and Hirschmann [61], partial melting of dry peridotite occurs in the sole presence of sulfide liquid at temperatures above the MSS liquidus. For example, at 1.5 GPa (equates to melting depth of ~45 km) and a mantle potential temperature of ~1350°C (which is typical for MORB mantle, e.g., [62]), sulfur is present as sulfide liquid. At the same pressure (1.5 GPa), MSS becomes stable at temperatures of ≤1200°C. In our melting model, we therefore use 1350°C and 1200°C at 1.5 GPa to simulate high-temperature sulfide melting in the presence of sulfide liquid (Fig. 4 light red an orange fields) and low temperature melting in the presence of MSS, respectively (cf. Fig. 4 (blue field) and Supplementary File 4). Below we will discuss the comparison of the results from the modeling with Au/Cu and Ag/Cu values in the natural samples from the Kermadec arc system starting with the evaluation of the low-T scenario. As low degree melts formed in the presence of MSS have much higher Ag/Cu values than Au/Cu, we will focus on Ag/Cu in the following paragraph.

Most Kermadec glasses show Ag/Cu values similar to those for mid-ocean ridge glasses. Four glasse samples from Kibblewhite, Kuiwai, Rumble V and the Havre Trough, however, have Ag/Cu values slightly higher than MORB. According to our model, ~7-10% sulfide melting in the presence of predominantly MSS at lower temperatures could explain the observed Ag/Cu values in these glasses. Three high-Mg andesite glasses from Kibblewhite, however, have high Ag/Cu of ~$6*10^{-5}$ that could be explained by ≤5% sulfide melting in the presence of MSS. Hirai et al. [36] proposed that the Kibblewhite high magnesian andesites formed via low-pressure melting (~1 GPa) of hydrous peridotite in the uppermost mantle beneath thin Kermadec arc crust at temperatures of ~1200°C. According to Zhang and Hirschmann. [61], partial melting of hydrous peridotite at low pressures at ~1200°C occurs in the sulfide liquid stability field. Partial melting in the presence of MSS seems, therefore, rather unlikely. The high magnesian Kibblewhite glasses plot intermediate between more mafic glasses from Kibblewhite with low Ag/Cu and siliceous melts with high Ag, high Ag/Cu values and low wt.% FeO^t, which can also plausibly be explained by magma mixing between ascending mafic and siliceous melts (cf. Fig. 2a and Fig. 2c). We therefore favor magma mixing to explain high Ag and Ag/Cu in the Kibblewhite high-magnesium andesitic glasses. Although very minor occurrence of low-degree melting in the presence of MSS seems reasonable, most of the Kermadec arc glasses have MORB-like Ag/Cu, which suggests that low-degree and low-temperature melting in the presence of MSS plays only a minor role in the Kermadec subarc mantle. This is consistent with published thermal models that predict rather high maximum mantle temperatures

ranging from 1380˚C to 1450˚C (model D80) [64] beneath the Kermadec arc front. Such temperatures are also consistent with predominantly partial melting in the presence of SL. Next, we will focus on the high-T scenario.

At 1.5 GPa and 1350°C in the presence of sulfide liquid, mantle sulfides are completely consumed when the degree of partial melting exceeds ~18 %. At higher degrees of partial melting (e.g., 20-25 %), Au/Cu and Ag/Cu in the natural samples will approach and eventually reflect that of the mantle source (cf. Fig. 4 and Supplementary File 3). However, degrees of partial melting of ≤ 18 % at high-temperatures and thus the sole presence of sulfide liquid explains most of the MORB data and some moderately mafic glasses from Giggenbach, Healy, Rumble II West, Brothers and the Havre Trough back-arc (Fig. 4, light red field), thus failing to account for high Au/Cu values of the remaining glasses.

Preferential incorporation of Cu over Au in low degree partial melts (i.e. <10%) at high temperatures results in higher Au/Cu in the residual mantle (cf. Fig. 4, light orange field). Therefore, a subarc mantle that underwent previous melt extraction has higher Au/Cu than depleted mantle. Gold to Cu ratios (at MORB-like Ag/Cu) in glasses from Monowai and Putoto (northern Kermadec arc) and from Rumble III, Giggenbach, Kuiwai, Kibblewhite, Ngatoroirangi and some near arc front glasses from the Havre Trough are higher than those of depleted mantle and MORB. The highest Au/Cu of up to $6*10^{-6}$ (~2 x higher than in primitive mantle) is observed in moderately mafic glasses from the northern Kermadec arc volcano Putoto. These glasses also have the lowest Nb/Zr (and Zr/Hf and whole rock $^{143}Nd/^{144}Nd$) suggesting their formation from the most depleted subarc mantle and/or through high degrees of melting. A depleted, hydrous subarc mantle that underwent ca. 5 % previous melt extraction has also been proposed to explain the fluid-immobile trace element distribution at Monowai located ~200 km to the north (e.g., [65]). Simililarly high Au/Cu of $>5.5*10^{-6}$ at intermediate Ag/Cu values are found in glasses from Kibblewhite, Ngatoroirangi and nearby Havre Trough. These glasses also have intermediate Nb/Zr requiring remelting of less depleted mantle than glasses to the north. Alternatively, high Au/Cu can be generated by incomplete pooling of partial mantle melts, assuming that low-degree melts (i.e. <10%) are extracted from the mantle and, for example, solidified during ascent. However, single remelting up to 18% of a previously depleted mantle cannot reproduce $Au/Cu*10^{-6}$ higher than $\sim5.4*10^{-6}$, requiring a second-stage of sulfide melt removal (cf. Fig. 4).

Low-degree second-stage melting at high temperature in the presence of sulfide liquid can reproduce the high Au/Cu in the Putoto, Ngatoroirangi, Kibblewhite and Havre Trough glasses at intermediate Ag/Cu values (Fig. 4, light orange field). Two-stage melt depletion has also been invoked to explain high Pt/Ru (which show similar melting behavior to Au/Cu) in the most depleted mantle at the Fonualai spreading center in the Lau Basin [18] and Pt/Ru ratios in boninites [8]. In addition, the Au content in the global lithospheric mantle ranges from 1.0 to 3.3 ppb and is generally highest in shallow lithospheric peridotites that underwent previous partial melting [66].

Taken together, the Au, Ag and Cu data from the Kermadec arc glasses require Au-Ag-Cu systematics that are different from that in MORB. Almost all the Kermadec arc glasses require high temperature

melting of variably depleted hydrous subarc mantle in the presence of sulfide liquid. Furthermore, high Au/Cu values in about half of the samples requires re-melting of depleted mantle under hydrous fluid flux from the subducting plate. Low-temperature melting in the presence of MSS does not seem to play a significant role in the formation of Kermadec arc magmas and may only be required to explain a few glasses with high Ag/Cu at intermediate Au/Cu. Partial melting in the stability field of MSS, however, may be more important at active continental margins with thickened crust and a colder mantle wedge, where it can be recognized based on elevated Ag/Cu in primitive melts. In summary, elevated mantle potential temperature driving multiple melting stages of highly depleted mantle and the availability of hydrous fluids appear to be the main factors controlling the Au content in primitive Kermadec magmas and possibly parental arc magmas globally.

Methods

Volcanic glasses analyzed in this contribution have been collected during seven surveys over the last 20 years with R/Vs *Tangaroa* (NZAPLUME I-III (1999-2004); NZASMS (2011); NIRVANA (2012); *Ka-imikai-o-Kanaloa* (NZASRoF'05 in 2005) and *Sonne* (SO255 Vitiaz in 2017) using rock dredges and the submersible Pisces. Sample locations and water depth for each sample are listed in Table 1.

Most of the 67 samples were taken from pillow rim glasses and some from glassy groundmass. Following sample crushing, fresh glass chips were handpicked and washed repeatedly in deionized water using an ultrasonic bath. Individual glass chips were then mounted in EpoThin (Buehler) epoxy-resin and the stubs polished using a sequence of increasingly fine-grained sand paper, diamond pastes and finally 0.05µm Al_2O_3 powder.

Major element and S, Cl and F contents were determined via electron micro-probe analyses (EMPA) at GEOMAR. The analyses were performed using a JEOL JXA8200 wave-length dispersive electron microprobe, conditions and reference materials as described by [67]. For trace elements, re-polished mounts (to remove the carbon coating required for the EMPA analyses) were analyzed with laser-ablation inductively coupled mass spectrometry (LA-ICPMS) at Institute of Geosciences, Kiel University. The analyses were performed using a quadrupole-based ICP-MS (Agilent 7900) and a ArF 193 nm Excimer LA system (Coherent GeoLas HD). In-situ micro-sampling was done with 160 µm pit size and 20 Hz pulse frequency at 10 J cm^{-2} fluence. Analyses were performed using a modified large volume ablation cell (LDHCLAC [68], ETH Zürich, Switzerland). The generated aerosol was transported with 0.75 L min^{-1} He and mixed with 0.6 L min^{-1} Ar prior to introduction into the ICP. The ICP-MS was operated under robust standard conditions at 1500W and optimized for low oxide and hydroxide formation (typically ThO/Th ≤ 0.4% and ThOH/Th≤ 0.05% monitored during entire analytical sessions at 248 m/z and 249 m/z). Sixty-five major and trace elements were analyzed on one spot. Analysis included 60 s instrumental background measurement (laser-off) and 60 s signal collection during laser ablation. Dwell time was 40 ms for Se, Ag, Re, Ir, Pt, Au, Tl and Bi and 1 ms for all other elements. One analytical cycle lasted 0.649 s; complete analysis comprised data from 180 cycles. Analytical signal on two mass-

numbers was collected for Cu (63, 65), Ag (107, 109), Re (184, 185), Ir (191, 193), and Pt (194, 195); one mass-number for all other elements. Initial data reduction was performed using Glitter software package [69] for setting time-resolved integration windows and initial non matrix-matched calibration using SRM-NIST612 glass [70] and Ca as internal standard. The subsequent data reduction and matrix-matched calibration was done in Microsoft Excel using in-house made tables. On the first step, correction for isobaric interferences has been applied for Se, Ag, Re, Ir, Pt and Au. For elements in focus of this work – Ag and Au – measured intensities were corrected for interferences of $^{91}Zr^{16}O$ on ^{107}Ag, $^{93}Nb^{16}O$ on ^{109}Ag and $^{181}Ta^{16}O$ on ^{197}Au. To measure the oxide production rates on masses of interest we analyzed in every analytical block of 20 points pantellerite glass - in house reference glass PANT from Pantelleria Island. This glass was chosen as the best one for corrections based on many years of experience with minerals, natural glasses and glasses artificially doped with some elements, because this glass is highly evolved and extremely enriched in all incompatible elements including Zr (2700 ppm), Nb (310 ppm), and Ta (18.6 ppm), and also equilibrated at oxygen-reduced conditions and is sulfide saturated, providing strong depletion in strongly siderophile and chalcophile elements, especially heavy PGE and Au. The glass contains 0.13 ppm Ag (obtained by numerous replicate analyses of Ag using mass 107 and natural zircon to estimate Zr/ZrO rate) and negligible (not detected and assumed to be 0 ppm) amounts of Au. The accuracy of the applied correction is confirmed by equal concentrations obtained for different isotopes (e.g., Ag on 107 and 109 m/z) and also by intercepts of calibration lines close to zero. The data corrected for interferences were then corrected for instrumental drift using NBS NIST612 (S, Se, Cd, In, As, Ag, Sb, Re, Pt, Au, Tl, Bi) and BCR-2G (all other elements) glasses. The final matrix-matched calibration was based on a series of 20 whole-rock international reference materials prepared as nano-particulate powder pellets (NPP) for direct in situ-analysis by laser ablation [71] and MPI-DING glasses [72] using recommended values from the GeoRem data base (http://georem.mpch-mainz.gwdg.de). During the final step, true concentrations were calculated by matching the sum of major element oxides to 100 wt.%[73-74]. NPP BHVO-2 and TDB-1 and MPI-DING glasses (KL2-G, GOR128-G) were analyzed as unknowns in the course of this study for checking long-term stability of the calibration and comparison with other studies (Supplementary File 3).

Typically, each glass sample was analyzed at 4 to 6 spots. Owing to the large beam-diameter of 160mm, ablation of microlites was inevitable for some samples. When a significant range of compositions was obtained due to variable entrapment of microliths, the data were corrected to obtain pure glass composition using regressions versus K_2O measured by LA-ICP-MS, extrapolated to K_2O from separate EPMA data. Where LA-ICP-MS data revealed no statistically significant trends and clustered near constant values within analytical uncertainty, the data were averaged and treated as the composition of the bulk ground mass (Table 1).

Accuracy of analyses is estimated from calibration lines as average relative deviation of data for reference materials from their recommended values to be 10% relative for Se (calibration range of 0.027-0.351 ppm, number of reference samples N=8), Au (0.7-6.3 ppb, N=5) and Ag (24-139 ppb, N=9) and 5% for Cu (18.6-343 ppm, N=13). Analytical detection limits for Se, Ag and Au are dependent on instrument

sensitivity and also on the amount of interfering oxides and were estimated to be ~0.02 ppm for Se, ~1 ppb for Ag and ~0.2 ppb for Au in Kermadec arc samples, which are depleted to moderately enriched in middle REE, Zr, Nb and Ta. The total uncertainty at 95% CL was estimated by using the error propagation rule as square root of sum of squared long-term accuracy of standard measurements and squared two relative standard deviation of sample replicate measurements.

Declarations

Acknowledgements

We thank the captains and members of the crew of the R/Vs *Tangaroa*, *Ka'imikai-o-Kanaloa* and *Sonne* for expert handling of the ships and equipment, and the pilots of *Pisces V* for enabling diverse sampling to be accomplished. We thank Henry Gard and Matthias Witte for their help preparing the samples and Mario Thöner and Ulrike Westernströer for analytical support and expertise. Discussions with Fabio Caratori Tontini, Steve Peircy, Yoshihiko Tamura and Jim Gill helped to shape the ideas. SO255 samples were collected using grant #03G0255A for the SO255-Vitiaz project funded by the German Federal Ministry of Education and Research (BMBF) and GEOMAR. CdR have been funded from grants made by the New Zealand Ministry of Business, Innovation and Education to GNS Science. This work was funded by the European Union's Horizon 2020 research and innovation program under the Marie Skłodowska-Curie grant agreement #79308 to CT.

Author contributions

CT and MP developed the idea and CT wrote the ms. MP developed the analytical protocol and produced the data together with CT. CdR, MH, KH, PB and ML contributed to the writing and clarification of the proposed model. CT, MP, CdR, KH conceived, got funding for and carried out the ship expeditions. DGS, DLM and RA contributed additional data and input to the ms.

Competing interests

The authors declare no competing financial interests.

References

1. Sillitoe, R.H., 1973, The tops and bottoms of porphyry copper deposits: Economic Geology 68, 799-815.
2. De Ronde, C.E.J., Baker, E.T., Massoth, G.J., et al., 2007, Submarine hydrothermal activity along the mid-Kermadec arc, New Zealand: large-scale effects on venting. Geochemistry, Geophysics, Geosystems 8 (7), Q07007, doi:10.1029/2006GC001495.
3. Richards, J.P., 2011, Magmatic to hydrothermal metal fluxes in convergent and collided margins: Ore Geology Review 40 (1), 1-26.

4. Timm, C., de Ronde, C.E.J., Leybourne, M., Layton-Matthews, D., Graham, I.J., 2012, Sources of chalco- and siderophile elements in Kermadec arc lavas. Economic Geology 107, 1527-1538.
5. Mungall, J.E., 2002. Roasting the mantle: Slab melting and the genesis of major Au and Au-rich Cu deposits. Geology 30 (10), 915-918.
6. Jenner, F.E., O'Neill, H.C.S., Arculus, R.J., and Mavrogenes, J.A., 2010, The magnetite crisis in the evolution of arc-related magmas and the initial concentration of Au, Ag and Cu. Journal of Petrology 51, 2445-2464.
7. Jenner, F.E., Arculus, R.J., Mavrogenes, J.A., Dyriw, N.J., Nebel, O., Hauri, E., 2012a, Chalcophile element systematics on volcanic glasses from the northwestern Lau Basin. Geochemistry, Geophysics, Geosystems 13 (6), Q06014, doi:10.1029/2012GC004088
8. Hamlyn, P.R., Keays, R.R., Cameron, W.E., Crawford, A.J., Waldron, H.M., 1985. Precious metals in magnesian, low-Ti lavas: Implication on metallogenesis and sulfide saturation in primary magmas. Geochimica et Cosmochimica 49, 1797-1811.
9. Keays, R.R. (1995) The role of komatiitc and picritic magmatism ans S-saturation in the formation of ore deposits. Lithos 34, 1-18
10. Zajacz, Z., Candela, P.A., Piccoli, P.M., Sanchez-Valle, C., Wälle, M. 2013. Solubility and partitioning behaior of Au, Cu, Ag and reduced S in magmas. Geochimica et Cosmochimica Acta 112, 288-304.
11. Botcharnikov, R.E., Linnen, R.L., Wilke, M., Holtz, F., Jugo, P.J., Berndt, J. 2011. High gold concebtrations in sulphide-bearing magma under oxidizing conditions. Nature Geoscience 4, doi:10.1038/NGEO1042.
12. Li, Y., Audedat, A., 2012. The partioning of V, Mn, Co, Ni, Cu, Zn, As, Mo, Ag, Sn, Sb, W, Au, Pb and Bi between sulfide phases and hydrous basanite melt at upper mantle conditions. Earth and Planetary Science Letters 355-356, 327-340.
13. Li, Y., Audedat, A., 2015. Effects of temperature, silicate melt composition, and oxygen fugacity on the partitioning of V, Mn, Co, Ni, Cu, Zn, As, Mo, Ag, Sn, Sb, W, Au, Pb, and Bi between sulfide phases and silicate melt. Geochimica et Cosmochimica Acta 162, 25-45.
14. Lee, C.-T., Luffi, P., Chin, E.J., Bouchet, R., Dasguptsa, R., Morton, D.M., Le Roux, V., Yin, Q.-z., Jin, D., 2012, Copper systematics in arc magmas and implications for crust-mantle differentiation. Science 336, 64-68.
15. Ding, S., Dasgupta, R., 2017. The fate of sulfide during decompression melting of peridotite – implications for sulfur inventory of the MORB-source depleted upper mantle. Earth and Planetary Science Letters 459, 183-195.
16. Arndt, N., Lesher, C.M., Czamanske, G.K., 2005, Mantle-derived magmas and magmatic Ni-Cu-(PGE) deposits. Economic Geology 100, 5-24.
17. Hamlyn, P.R., Keays, R.R., 1986, Sulfur Saturation and second-stage melts; application to the Bushveld platinum metal deposits. Economic Geology 81, 1431-1445.
18. Dale, C.W., Macpherson, C.G., Pearson, D.G., Hammond, S.J., Arculus, R.J. 2012. Inter-element fractionation of highly siderophile elements in the Tonga arc due to flux melting of a depleted

source. Geochimica et Cosmochimica 89, 202-225.

19. Prokovsky, G.S., Kokh, M.A., Guillaume, D., Borisove, A.Y., Gisquet, P., Hazemann, J.-L., Lahera, E., Del Net, W., Proux, O., Testemale, D., Haigis, V., Jonchiere, R., Seitsonen, A.P., Ferlat, G., Vuilleumier, R., Saitta, A.M., Boiron, M.-C., Dubessy, J., 2015. Sulfur radical species form gold deposits on Earth. Proceeding of the National Academy of Sciences 112 (44), 13484-13489, doi: 10/1073/pnas.1506378112.
20. Kepezhinskas P, Defant MJ, Widom E (2002) Abundance and distribution of PGE and Au in the island-arc mantle: implications for sub-arc metasomatism. Lithos 60:113-128
21. Smith, W.H.F, Sandwell, D.T. 1997. Global sea floor topography from satellite altimetry and ship depth soundings. Science 277, 1956-1962. Doi:10.1026/science.277.5334.1956.
22. DeMets, C., Gordon, R.G., Argus, D.F., Stein, S., 1994. Effects of recent revisions to the geomagnetic reversal time scale on estimates of current plate motions. Geophysical Research Letters 21 (20), 2192-2194.
23. de Ronde, C.E.J., Baker, E.T., Massoth, G.J., Lupton, J.E., Wright, I.C., Feely, R.A., Greene, R.R, 2001. Intra-oceanic subduction-related hydrothermal venting, Kermadec volcanic arc, New Zealand. Earth and Planetary Science Letters 193, 359-369.
24. de Ronde, C.E.J., Massoth, G.J., Butterfield, D.A., et al., 2011, Submarine hydrothermal activity and gold-rich mineralization at Brothers volcano, Kermadec arc, New Zealand: Mineralium Deposita, doi 10.1007/s00126-011-0345-8.
25. Sillitoe, R.H., 2020, Gold deposit types: an overview. In Geology of the World#s major gold deposits and provinces. Special Publications of Economic Geologists, 1-28.
26. de Ronde, C.E.J., Walker, S., Ditchburn, R.G., et al., 2014, The Anatomy of a buried submarine hydrothermal system, Clark volcano, Kermadec Arc, New Zeland. Economic Geology 109, 2261-2292.
27. de Ronde, C.E.J., Humphris, S.E., Höfig, T.W., Reyes, A.G., and the IODP Expedition 376 Scientists, 2019. Critical role of caldera collapse in the formation of seafloor mineralization: The case of Brothers volcano. Geology 47, 762-766, https://doi.org/10.1130/G46047.1
28. Hayes, G.P., Moore, G.L., Portner, D.E., Hearne, M., Flamme, H., Furtney, M., Smocyk, G.M. 2018. Slab2, a comprehensive subduction zone geometry model. Science 362, 58-61.
29. Bassett, D., Kopp, H., Sutherland, R., Henrys, S., Watts, A.B., Timm, C., Scherwath, M., Grevemeyer, I. de Ronde, C.E.J., 2016. Crustal structure of the Kermadec arc from MANGO seismic refraction profiles. Journal of Geophysical Research 121, doi:10.1002/2016JB013194.
30. Hoernle, K., Hauff, F., Bogaard, Pvd., Werner, R., Mortimer, N., Geldmacher, J., Garbe-Schoenberg, D. & Davy, B. Age and geochemistry of volcanic rocks from the Hikurangi and Manihiki oceanic Plateaus. Geochimica et Cosmochimica Acta 74, 7196–7219, doi:10.1016/j.gca.2010.09.030 (2010).
31. Timm, C., Davy, B., Haase, K., Hoernle, K.A., et al., 2014, Subduction of the oceanic Hikurangi Plateau and its impact on the Kermadec arc. Nature Communications 5:4923, doi:10.1038/ncomms5923

32. Gill, J., Hoernle, K., Todd, E., Hauff, F., Werner, R., Timm, C., Garbe-Schönberg, D., Gutjahr, M. 2021. Basalt geochemistry and mangle flow during early backarc basin evolution: Havre Trough and Kermacec arc, Southwest Pacific. Geochemistry Geophysics Geosystems 22, e2020GC009339. Doi:10.1029/2020GC009339.
33. Wysoczanski, R., Handler, M., Schipper, C.I., Leybourne, M., Creech, J., Rotella, M., Nichols, A., Wilson, C.J.N., Stewart, R.B., 2012. The tectonomagmatic source of ore metals and volatile elements in the southern Kermadec arc. Economic Geology 107, 1539-1556.
34. Haase, K.A, Stroncik, N.Garbe-Schönberg, D., Stoffers, P. 2006. Formation of island arc dacite magmas by extreme crystal fractionation: an example from Brothers Seamount, Kermadec island arc, New Zealand. Journal of Volcanology and Geotherm Research 152, 316-330.
35. Brandl, P., Portnyagin, M., Zeppenfeld, H., Tepley jr, F., de Ronde, C.E.J., Timm, C., Hauff, F., Garbe-Schönberg, D., Graham, I., Bosquet, R. 2022. The origin of magmas and metals at the submarine Brothers volcano, SW Pacific. Economic Geology, https://doi.org/10.5382/econgeo.4973
36. Hirai, Y., Tamura, Y., Sato, T., Miyazaki, T., Chang, Q., Vaglarov, B.S., Kimura, J.-I., Hoernle, K., Werner, R., Huaff, F., Timm, C. 2023. Magnasian Andesites from Kibblewhite volcano in the Kermadec arc, New Zealand. Journal of Petrology 64, 1-23, doi:10.1093/petrology/egad060.
37. O'Neill, H.S.C., Mavrogenes, J.A. 2002. The Sulfide Capacity and the Sulfur Content at Sulfide Saturation of Silicate Melts at 1400°C and 1 bar. Journal of Petrology 43 (6),1049-1087, doi:10.1093/petrology/43.6.1049.
38. Jenner, F.E., O'Neill, H., 2012b. Analysis of 60 elements in 616 ocean floor basaltic glasses. Geochemistry, Geophysics, Geosystems 13 (1), Q02005, doi:10.1029/2011GC004009.
39. Yang, S., Humayun, M., Salters, V.J.M., 2018. Elemental Systematics in MORB glasses from the Mid Atlantic Ridge. Geochemistry, Geophysics, Geosystems 19, 4236-4259, doi:10.1029/2018GC007593.
40. Wang, Z., Becker, H. 2015. Abundances of Ag and Cu in mantle peridotites and the implications for the behavior of chalcophile elements in the mantle. Geochimica et Cosmochimica Acta 160, 209-226.
41. Palme, H., O'Neill, H. 2014. Cosmochemical estimates of mantle composition. Treatise on Geochemistry, 2nd edition. 39 pp, doi:10.1016/B978-0-08-095975-7.00201-1
42. Gale, A., Daltin, C.A., Langmuir, C.H., Su, Y., Schilling, J.-G., 2013. The mean composition of ocean ridge basalts. Geochemistry Geophysics Geosystems 14, 489-518. Doi:10.1029/2012GC004334.
43. Workman, R., Hart, S. 2005. Major and trace element composition of the depleted MORB mantle (DMM). Earth and Planetary Science Letters 231, 53-72.
44. Salters, V.J.M., Stracke, A., 2004. Composition of depleted mantle. Geochemistry Geophysics and Geosystems 5 (5), Q05004, doi:10.1029/2003GC000597.
45. Prokovsky, G.S., Dubrovinsky, LS., 2011. The S_3^- ion is stable in geological fluids at elevated temperatures and pressures. Science 331, 1052-1054, doi: 10.1126/science.1199911.

46. Gamble, J., Woodhead, J., Wright, I., Smith, I., 1996. Basalt and sediment geochemistry and magma petrogenesis in a transect from oceanic island arc to rifted continental margin arc: the Kermadec-Hikurangi margin, SW Pacific. Journal of Petrology 37 (6), 1523-1546.
47. Turner, S., Hawkesworth, C., Rogers, N., Bartlett, J., Worthington, T., Hergt, J., Pearce, J., Smith, I. 238U-230Th disequilibria, magma petrogenesis, and flux rates beneath the depleted Tonga-Kermadec island arc. Geochimica et Cosmochimica Acta 61 (22), 4855-4884.
48. Timm, C., Leybourne, M.I., Hoernle, K., Wysoczanski, R.J., Hauff, F., Handler, M., Caratori-Tontini, F., de Ronde, C.E.J. 2016. Trench-perpendicular geochemical variations between two adjacent Kermadec arc volcanoes Rumble II E and West: the role of the subducted Hikurangi Plateau in element recycling in arc magmas. Journal of Petrology 57 (1), 1335-1360, doi:10.1093/petrology/egw042.
49. Pitcairn, I.K. 2011. Background concentrations of gold in different rock types. Applied Earth Science IMM Transaction section B 120 (1), 31-38. Doi: 10.1179/1743275811Y.000000021.
50. MacKay, J.L., Pedersen, T.F., 2008. The accumulation of silver in marine sediments: A link to biogenic Ba and marine productivity. Global Biochemical Cycles 22, GB 4010, doi: 10.1029/GB003136.
51. Plank, T., Langmuir, C. 1998. The chemical composition of subducting sediments and its comsequences for the crust and mantle. Chemical Geology 145 (3-4), 325-394.
52. Hannington, M., 2013. The role of black smokers in the CU mass balance of the oceanic crust. Earth and Planetary Science Letters 374, 215-226.
53. Fru, E.C., Rodriguez, N.P., Partin, C.A., Lalonde, S.V., Andersson, P., Weiss, D.J., El Albani, A., Rodushkin, I., Konhauser, K.O. 2016. Cu isotopes in marine black shales record the Great Oxidation Event. Proceedings of the National Academy of Science 113, 4941-4946, doi:10.1073/pnas.1523544113.
54. Plank, T., 2005. Constraints from Thorium/Lanthanum on sediment recycling at subduction zones and the evolution of the continents. Journal of Petrology 46 (5), 921-944.
55. Wallace, L, Saffer, D., Barnes, P., Pecher, I., Petronotis, K., LeVay, L. and the Expedition 372/375 Scientists, 2019. Hikurangi subduction margin coring, logging, and observatories. Proceeding of the International Ocean Discovery Program, 372B/375: College Station, TX (International Ocean Drilling Program), doi:10.14379/iodp.proc.372B375.2019.
56. Takashima, R., Nishi, H., Yamanaka, T., Tomosugi, T., Fernando, A.G., Tanabe, K., Moriya, K., Kawabe, F., Hayashi, K. 2011. Prevailing oxic environments in the Pacific Ocean during the mid-Cretaceous oceanic anoxic event 2. Nature Communications 2, Article number: 234.
57. Castillo, P.R., Lonsdale, P.F., Moran, C.L., Hawins, J.W. 2009. Geochemistry of mid-Cretaceous Pacific crust being subducted along the Tonga-Kermadec trench: Implications for the generation of arc lavas. Lithos 112, 87-102.
58. Davy, F., Hoernle, K., Werner, R., 2008. Hikurangi Plateau: Crustal structure, rifted formation, and Gondwana subduction history. Geochemistry Geophysics and Geosystems 9 (7), Q07004, doi:10.1029/2007GC001855.

59. Reekie, C.D., Jenner, F.E., Smythe, D.J., Hauri, E.H., Bullock, E.S., Williams, H.M., 2019. Sulfide resorption during ascent and degassing of oceanic plateau basalts. Nature Communications 10:82, doi:10.1038/s41467-018-08001-3.
60. Kessel, R., Schmidt, M.W., Ulmer, P., Pettke, T., 2005. Trace element signature of subduction-zone fluids, melts and supercritical liquids at 120-180 km depth. Nature 437, 724-727, doi:10.1038/nature03971.
61. Zhang, Z., Hirschmann, M. 2016. Experimental constraints on mantle sulfide melting. American Mineralogist 101, 181-192.
62. Green, D.H., Falloon, T.J., Eggins, S.M., Yaxley, G.M., 2001. Primary magmas and mantle temperatures. European Journal of Mineralogy 13 (3), 437-452.
63. Katz, R.F., Spiegelman, M., Langmuir, C.H., 2003. A new parameterization of hydrous mantle melting. Geochemistry, Geophysics, Geosystems 4 (9), 1073, doi:10.1029/2002GC000433.
64. Syracuse, E.M., van Keken, P.E., Abers, G.A., 2010. The global range of subduction zone thermal models. Physics of the Earth and Planetary Interiors 183, 73-90.
65. Timm, C., Graham, I., de Ronde, C.E.J., Leybourne, M., Woodhead, J., 2011. Geochemical evolution of Monowai volcanic center: New insights in the northern Kermadec arc system. Geochemistry, Geophysics, Geosystems 12 (8), Q0AF01, doi:10.1029/2011GC003654.
66. Saunders, J.E., Pearson, N.J., O'Reilly, S.Y., Griffin, W.L., 2018. Gold in the mantle: A global assessment of abundance and redistribution processes. Lithos 322, 376-391.
67. Ponomareva, V., Portnyagin, M., Pendea, I.F., Zelenin, E., Bourgeois, J., Pinegina, T., Kozhurin, A., 2017. A full Holocene tephrochronology for the Kamtchatsky Peninsula region: Applications from Kamchatka to North America. Quaternary Science Reviews 168, 101-122. Doi:10.1016/j.quasirev.2017.04.031.
68. Fricker, M. B., Kutscher, D., Aeschlimann, B., Frommer, J., Dietiker, R., Bettmer, J., Günther, D., 2011. High spatial resolution trace element analysis by LA-ICP-MS using a novel ablation cell for multiple or large samples. International Journal of Mass Spectrometry 307, 39–45.
69. Griffin, W.L., 2008. GLITTER: data reduction softwarefor laser ablation ICP-MS. In: Laser Ablation ICP-MS in the Earth Sciences: Current Practices and outstanding issues, 308-311.
70. Jochum, K.P., Weis, U., Stoll, B., Kuzmin, D., Yang, Q., Raczek, I., Jacob, D.E., Stracke, A., Birbaum, K., Frick, D., Günther, D., Enzweiler, J., 2011. Determination of reference values for NIST SRM 610-617 glasses following ISO guidelines. Geostandards and Geoanalytical Research 35, 397-429. Doi:10.111/j..1751-908X.2011.00120.x
71. Garbe-Schönberg, D., Müller, S., 2014. Nano-particulate pressed powder tablets for LA-ICP-MS. Journal of Analytical Atomic Spectrometry 29 (6):990-1000, doi:10.1039/c4ja
72. Jochum, K. P., et al. 2006, MPI-DING reference glasses for in situ microanalysis: New reference values for element concentrations and isotope ratios, Geochemistry Geophysics Geosystems 7, Q02008, doi:10.1029/2005GC001060.

73. Pettke, T., Halter, W. E, Webster, J. D., Aigner-Torres, M., Heinrich, C. A., 2004. Accurate quantification of melt inclusion chemistry by LA-ICPMS: a comparison with EMP and SIMS and advantages and possible limitations of these methods. Lithos, 78(4), 333-361, doi: 10.1016/j.lithos.2004.06.011.
74. Kimura, J.-I., Chang, Q., 2012. Origin of the suppressed matrix effect for improved analytical performance in determination of major and trace elements in anhydrous silicate samples using 200 nm femtosecond laser ablation sector-field inductively coupled plasma mass spectrometry. Journal of Analytical Atomic Spectrometry 27, 1549-1559, doi:10.1039/C2JA10344C.

Table

Table 1 is available in the Supplementary Files section

Figures

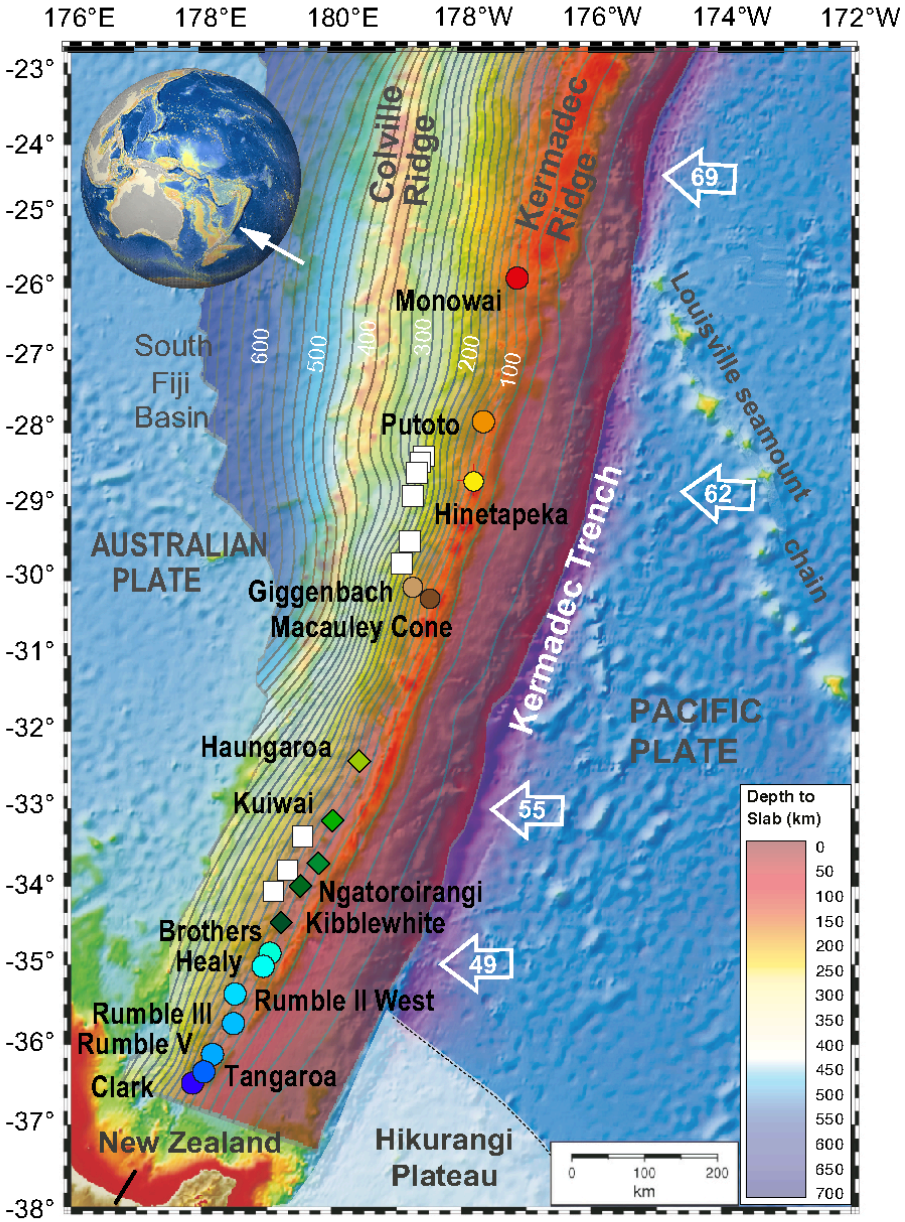

Figure 1

Bathymetric map after Smith and Sandwell [21] overlain by the USGS slab-surface model [28]. Inset shows a globe with the location of the Kermadec arc. Symbols mark sampled locations of Kermadec arc front volcanoes and Havre Trough back-arc. Grey lines mark slab depth contours spaced at 20 km. Arrows with numbers are subduction velocity rates after DeMets et al. [22].

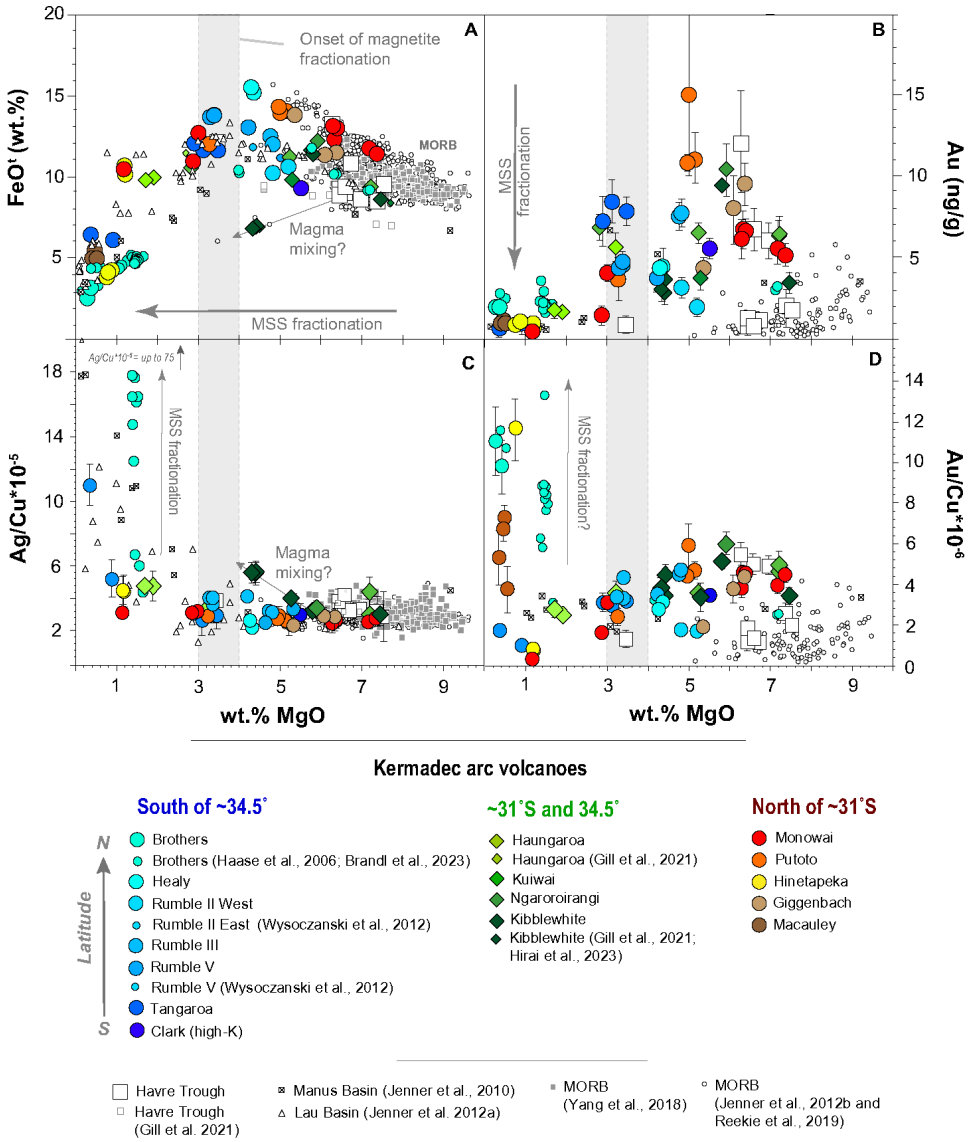

Figure 2

A) Concentration of MgO versus A) FeO^t, B) Au, C) Ag/Cu and D) Au/Cu. Kermadec arc literature data are from [32-36]. MORB = mid ocean ridge basalt [38-39]. All data sources are as listed in the legend.

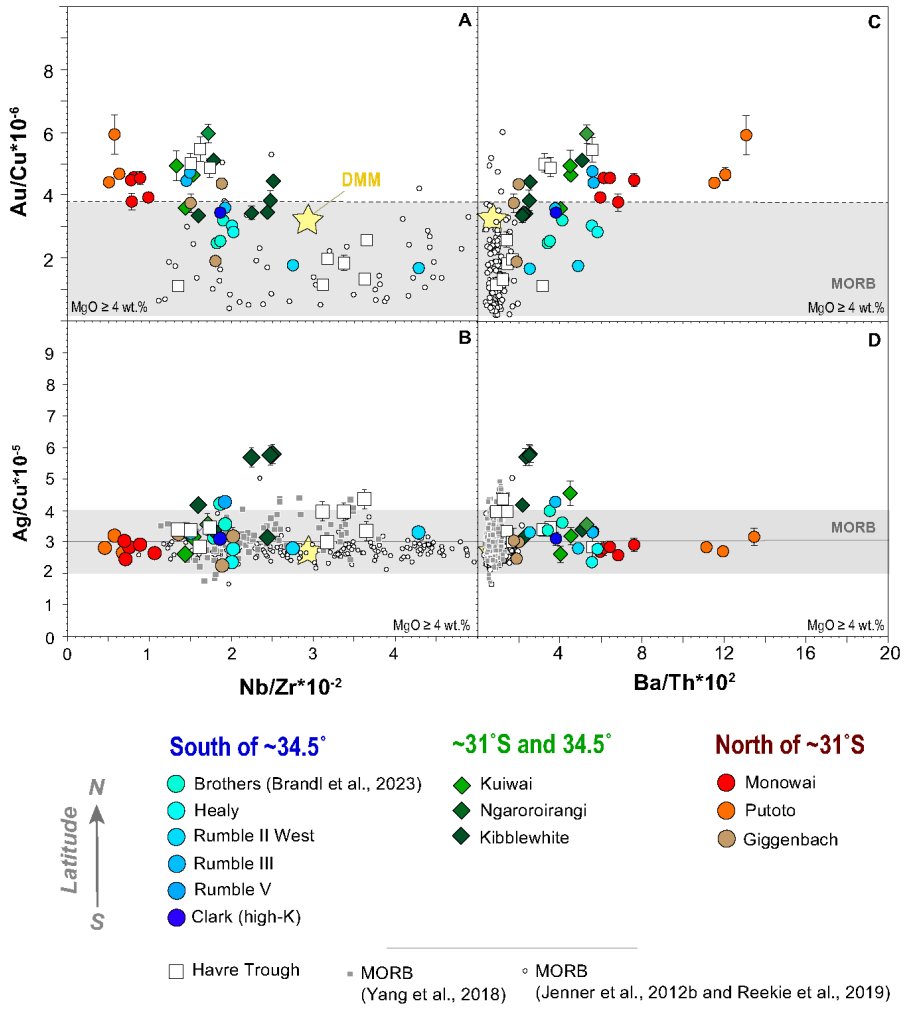

Figure 3

Panels A and B show Nb/Zr versus A) Au/Cu and B) Ag/Cu for Kermadec arc glasses with MgO > 4 wt.%. Panels C and D show Ba/Th versus Au/Cu and Ag/Cu, respectively. MORB: mid ocean ridge basalt data from [38-39, 42]. Depleted MORB mantle (DMM) is after [40] (Ag = 8 ppb and Cu = 30 ppm) and Au = 1 ppb and Cu = 30 ppm after [41] and Nb and Zr after [43] and Ba and Th after [44].

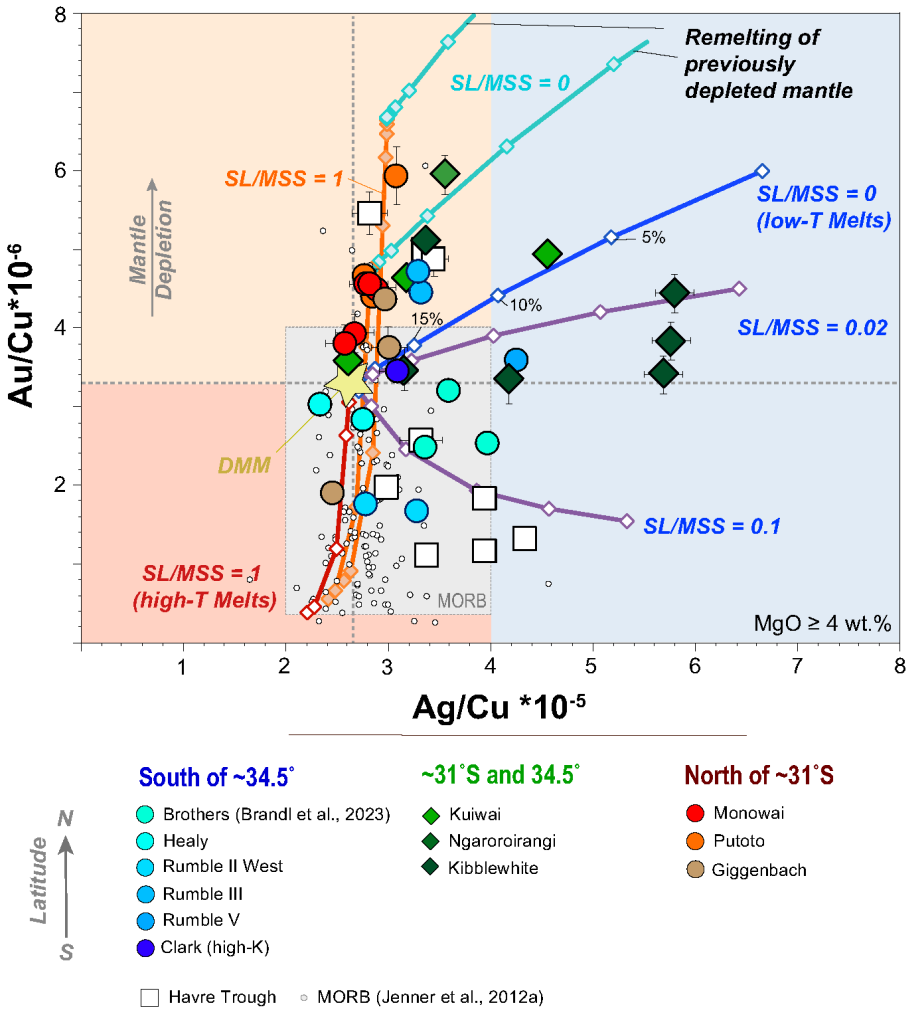

Figure 4

Ag/Cu versus Au/Cu of the Kermadec arc volcanic glasses (MgO > 4 wt.%). The red line represents the partial melting model of high-temperature sulfide liquid (SL) and blue line represents partial melting model of low-temperature mono sulfide solid solution (MSS). According to ref. [61] , partial melting of dry mantle occurs in the sole presence of sulfide liquid. Accordingly, we use a high melting temperature of T=1350°C at 1.5 GPa (equates to ~45 km subarc melting depth), oxygen fugacity set at +1 log units

above the quartz-fayalite-magnetite (QFM) buffer and the bulk mantle S content of 200 ppm S in our model. To model low temperature mantle melting we use 1200°C at 1.5 GPa (at QFM +1 and 200 ppm S), conditions under which MSS can be stable [61]. These conditions correspond to the conditions of the (hydrous) peridotite solidus in the presence of ~0.1% H_2O [63]. The purple lines are partial melting curves in the presence of SL and MSS. Symbols on the modelled trajectories are 5% melting increments. Orange line represents high-temperature remelting of previously depleted mantle in the presence of SL and the turquoise lines are trajectories of low temperature remelting of previously depleted mantle (each melting depletion event assumes 9% melt extraction). Depleted mantle values are after [40-41]. MORB data are from [38-39].

Supplementary Files

This is a list of supplementary files associated with this preprint. Click to download.

- TimmGoldMsSupplementaryFiles14.pdf
- TimmGoldMsSupplementaryFiles5.pdf
- Table1MajorsTracesNew.xlsx